ELSEVIER

Contents lists available at ScienceDirect

Applied Thermal Engineering

journal homepage: www.elsevier.com/locate/apthermeng



Research Paper

Experimental validation of numerical heat transfer models of an impingement jet at high Reynolds numbers[★]

Eileen Trampe*, Dominik Büschgens, Herbert Pfeifer, Christian Wuppermann

Department for Industrial Furnaces and Heat Engineering, RWTH Aachen University, Germany

ARTICLE INFO

Keywords: Heat transfer Convective heat transfer Impingement jet characteristics Particle Image Velocity Numerical Modelling

ABSTRACT

In industrial thermal processing plants, metal strips are quenched in cooling zones by impingement jets, with convection being the dominant heat transfer mechanism. To generate the impingement jets, gas is accelerated through a nozzle system and directed onto the material surface, resulting in rapid and uniform cooling. The present work involves the experimental investigation of the heat transfer and associated flow of impingement jets using PIV on a single slot (W=5 mm) and a single round nozzle (D=25 mm). These experimental methods form the basis for the evaluation of numerical turbulence models. The turbulence models selected in this work are: SST k- ω model, Generalised k- ω (GEKO) model and the Reynolds Stress Model. The investigations are carried out at a nozzle exit velocity of $u\approx51$ m/s ($Re_{Slot}=34,490$, $Re_{Round}=88.780$). Compared to other studies with a Reynolds number of below 23,000, the prediction accuracy is less due to the high Reynolds number. The PIV measurement shows that the flow velocities are correctly modelled, but the turbulent kinetic energy can only be poorly predicted. trampe@iob.rwth-aachen.de

1. Introduction

In continuous strip processing lines and chamber furnaces for the heat treatment of steel, aluminium, and copper strips, nozzle systems are used to heat or cool the strip using high velocity gas jets. Continuous annealing lines have an annual capacity of up to one million tonnes of steel strip fed vertically through the furnace. High-quality aluminium and copper strips are preferably heat-treated continuously in floating strip furnaces. The main advantage of these systems is their horizontal design, in which the strip is guided through the furnace without contact on the air cushions generated by the nozzles [1,2]. Fig. 1 presents examples of continuous annealing lines for steel strip.

In order to adjust the material properties for the subsequent application, a heat treatment following a predefined temperature over time cycle has to be achieved. Particular attention has to be paid on the necessary cooling rates. Depending on the thickness of the metal strips, cooling rates of up to 150 K/(s·mm) per millimetre of strip thickness s must be achieved [4]. With recirculated gas quenching (1000 mbar N₂) maximum heat transfer coefficients of 100 - 150 W/(m²K) can be reached. By adjusting process parameters such as increasing the flow velocities, the heat transfer coefficients can approach values up to

 $300 - 400 \text{ W(/m}^2\text{K)}$ [5]. This technology can therefore be flexibly adapted to the process. The nozzle systems are aimed at the strip in such a way that the resulting impingement jet ensures the highest possible and most homogeneous heat transfer. The heat transfer between the strip and the fluid is dominated by convection. To assess the heat transfer behaviour of the impingement jet, a heat transfer coefficient h is defined and represented dimensionless by the Nusselt number Nu, Eq. (1) [6,7].

$$Nu = \frac{h \cdot D_h}{\lambda} = f(Re, Pr, Geometry) \text{ with } h = \frac{\dot{q}}{T_{Strip} - T_{Fluid}}$$
 (1)

The Nusselt number describes the cooling or heating rate of the strip. A higher Nusselt number ensures a better heat transfer between the fluid and the strip, leading to a faster cooling or heating. A number of factors such as nozzle exit velocity u, strip distance H, fluid properties and nozzle geometry (round nozzle: diameter D, slot nozzle: nozzle width W) affect the heat transfer coefficient of impingement jets. Typically, nozzle fields consisting of round or nozzles are used in thermal processing plants [8].

Due to the high degree of flexibility in the application of impingement jets, it has already been the subject of several studies. Experimental investigations on slot nozzle systems were carried out as early as 1965

E-mail address: trampe@iob.rwth-aachen.de (E. Trampe).

 $^{^{\}star}$ This article is part of a special issue entitled: 'Conference ExHFT-10' published in Applied Thermal Engineering.

^{*} Corresponding author.

Nomenclature		p	pressure [Pa]
		ρ	fluid density [kg/m³]
D	nozzle diameter [mm]	q	heat flux density $[W/m^2]$
D_h	hydraulic diameter [mm]	Q'	heat flux [W]
ε	uncertainty [%]	Re	Reynolds number [-]
H	strip distance [mm]	S	spacing, nozzle-to-nozzle distance [mm]
h	heat transfer coefficient $[W/(m^2K)]$	и	fluid velocity $[m/s]$
k	turbulent kinetic energy (TKE) $[m^2/s^2]$	T	temperature [K]
μ	dynamic viscosity [Pa·s]	t	thickness [mm]
L	nozzle length [mm]	W	nozzle width [mm]
λ	thermal conductivity [W/(mK)]	Φ	heat generation $[W/m^3]$
ν	kinematic viscosity $[m^2/s]$	ω	specific turbulence dissipation rate $[s^{-1}]$
Nu	Nusselt number [-]	у	wall distance [mm]
PIV	particle Image Velocimetry [-]	\mathbf{v}^+	dimensionless wall distance [-]

by Hilgeroth (W=15-50 mm, Re=4,000-30,000) [9], and further investigations on the fundamentals of heat transfer from impingement jets to slot nozzle systems were done by Martin ($W=10\,$ mm, Re=3,000-90,000) [10]. In the context of heat transfer in industrial furnace technology, slot nozzle systems were investigated by Menzler ($W=6-25\,$ mm, Re=5,260-65,700) [11]. The focus of his work is the identification of geometric and fluidic influences on heat transfer in slot nozzle systems.

Numerous tests were carried out on round nozzle systems before the turn of the millennium [9,10,12–14]. More recent work has been carried out on round nozzle systems by Katti [15], Rao [16], O'Donovan [17] and Alimohammadi [18]. Due to the large number of investigations, the effects of the H/D ratio, the s/D ratio and the different Reynolds numbers investigated are well known. A high-resolution method for determining the heat transfer of industrial nozzle systems was presented by Trampe and Rademacher [19]. In addition to earlier studies, it is possible to determine the heat transfer on the strip surface per 1.28 mm² and to analyse nozzle systems with Reynolds numbers Re > 100,000 with the same accuracy.

The data collected in these experimental studies provide the basis for empirical equations to calculate the Nusselt number, which afterwards can be used to design nozzle systems for thermal processing plants [20]. However, these equations have the disadvantage that they can only be used in a limited Reynolds number range due to the conditions and parameter variations during the experiments. The experimental conditions are often exceeded due to the large-scale equipment used in thermal process technology (Re > 30,000). Another limitation is that the most Nusselt number relations only predict an average value, applicable integrally to the entire cooling zone. However, for the successful heat

treatment of metallic strip, accurate knowledge of the local Nusselt number is of great importance in order to ensure homogeneous material properties throughout the strip.

The detailed design of these systems using numerical modelling plays an increasingly important role. This is confirmed by the large number of numerical studies that have been carried out, with the high level of turbulence posing a particular challenge [21]. A comprehensive summary of the current state of numerical modelling of impact flows can be found in Zuckerman [22]. Table 1 summarises numerical investigations of impingement jets on single slot nozzles, while Table 2 shows the same for single round nozzles. The focus here is on Reynolds Averaged Navier Stokes (RANS) based solutions. Direct Numerical Simulations (DNS) is out of question due to the high Reynolds numbers and Large Eddy Simulation (LES) is too computationally intensive to be a suitable

Table 1Numerical studies on determining the heat transfer for SSN.

Author (Year)	H/ W	Re	Turbulence model
Benmouhoub (2014)	8	10,000 – 25,000	k-w
Achari (2017) [24]	6	15,000	k-ε
Pawar (2018) [25]	7.5	9,900	k-ε
Kadiyala (2019) [26]	2	100 - 5,000	SST-k-ω
Barata (2023) [27]	4	20,000	k - k l- ω Transition, SST k - ω , Transition SST, Realizable k - ε , RSM
Menzler (2023) [28]	5	66,000	SST k - ω , Generalised (GEKO) k - ω



Fig. 1. Examples of continuous annealing lines for steel strip: (a) two annealing furnaces in full view and (b) detailed view of the strip accumulator [3].

Table 2Numerical studies on determining the heat transfer coefficient for SRN .

Author (Year)	H/D	Re	Turbulence model
Draksler (2011) [33]	2	23,000	SST k-ω
Alimohammadi (2014) [18]	1.0 – 6.0	6,000 – 14,000	k - ε , RNG k - ε , k - ω , SST k - ω
Petera (2015) [34]	2, 6	23,000	SST k-ω, k-kl-ω Transition
Barbosa (2020) [29]	_	2,000	SST k - ω
Chitsazan (2022) [35]	2	23,000	SST k - ω
Rasheed (2022) [36]	0.5 –	20,000	SST k - ω , k - ω , Generalised
	6.0		(GEKO) k – ω ,
			BSL k – ω , k - kl - ω Transition,
Yüksedağ (2024) [32]	2	23,300	Generalised (GEKO) k – ω

method for manufacturers and operators of thermal processing plants.

The investigations listed in Table 1 show that the focus of previous investigations on slot nozzles has been predominantly on Reynolds numbers < 25,000. An exception is the investigation of a slot nozzle at Re=66,000 by Menzler, which is also characterised by the fact that the numerical results themselves have been experimentally validated. All other studies were validated using results from other authors. The studies [23–26] show good agreement between experimental data and numerical results, while Barata [27] and Menzler [28] describe large deviations. No further studies have been found on the investigation of slot nozzles where the airflow directly hits a steady flat surface. As a result, there is still no widely accepted numerical method for predicting the heat transfer of single slot nozzles with high accuracy for impingement jets at high Reynolds numbers.

A similar scenario is seen in the numerical analysis of single round nozzles. Either very low Reynolds numbers are investigated [18,29] or a Reynolds number of Re=23,000. This Reynolds number is often analysed numerically, as Baughn's experimental work is always used as a basis for validation [30,31]. The most accurate results were obtained with the SST k- ω and the lowest with k- ε variants. Yüksedağ [32] went one step further and optimised the Generalised (GEKO) k- ω turbulence model by adjusting the GEKO parameters for a single round nozzle with Re=23,300, resulting in higher accuracy.

The purpose of this paper is to establish and verify a RANS method for accurately predicting the local Nusselt number for a slot and round steady impinging jet, using our own experimental measurements for validation. The experimental validation is divided into two parts. The high-resolution determination of the Nusselt number and the

visualisation of the flow with Particle Image Velocimetry (PIV). The overall aim is to find a turbulence model that predicts the local Nusselt number within 5 % of error. This is an ambitious goal in view of the extensive work done by other authors, but it can be achieved by modifying the most promising turbulence model. To do so, it is necessary to analyse the initial flow situation for typical boundary conditions in thermal process plants and to consider the advantages and disadvantages of the respective turbulence models.

2. Experimental methodology

The experimental investigations for a complete examination of the impingement jet characteristics are divided into two parts. In the first part, the mean and local Nusselt number of an individual nozzle are determined. This is followed by analysis of the flow characteristics using the non-contact optical measurement method PIV to visualise the impingement jet. The experimental setup for analysing the convective heat transfer of the impingement jets consists of a fan, an inlet section with a volume flow measurement, a distribution chamber, a variable nozzle array and a conductively heated strip with 0.63 x 1.16 m 2 , Fig. 2. The total size of the test rig is 8 x 5 x 4 m 3 (length x width x height).

Ambient air is drawn in by the fan, which allows a maximum pressure increase of $\Delta p=22,800$ Pa at a maximum fan speed of r=3000 min⁻¹. The fan is connected to the distribution chamber with a tube. A Wilson measurement grid for the volumetric flow measurement is incorporated into the tube. Various nozzle systems can be easily mounted on the distribution chamber to investigate different nozzle geometries and nozzle pitches s to the heat transfer. The distribution chamber has a maximum mounting area for nozzle fields of 1480 x 1560 mm². Above the nozzle field a conductively heated strip with an area of 630 x 1160 mm² representing the impingement surface is positioned. The strip is heated by resistance heating using three transformers with an electrical power of P=12.5 kVA each until a stationary state is reached. The conductive heating strip is a constantan® strip (CuNi44, $\lambda=21.5$ W/(mK)) which is heated up to 600 °C.

The distance H between the strip and the nozzle array can be adjusted in the range of H=0–250 mm. During the measurement of the heat transfer, an impingement jet causes a convective heat transfer that cools the strip locally. This, together with the electrical resistance heating of the strip, creates a specific temperature field. This temperature field is measured using an infrared thermal camera. Based on the energy balance for each pixel the heat transfer coefficient is derived, Eq.

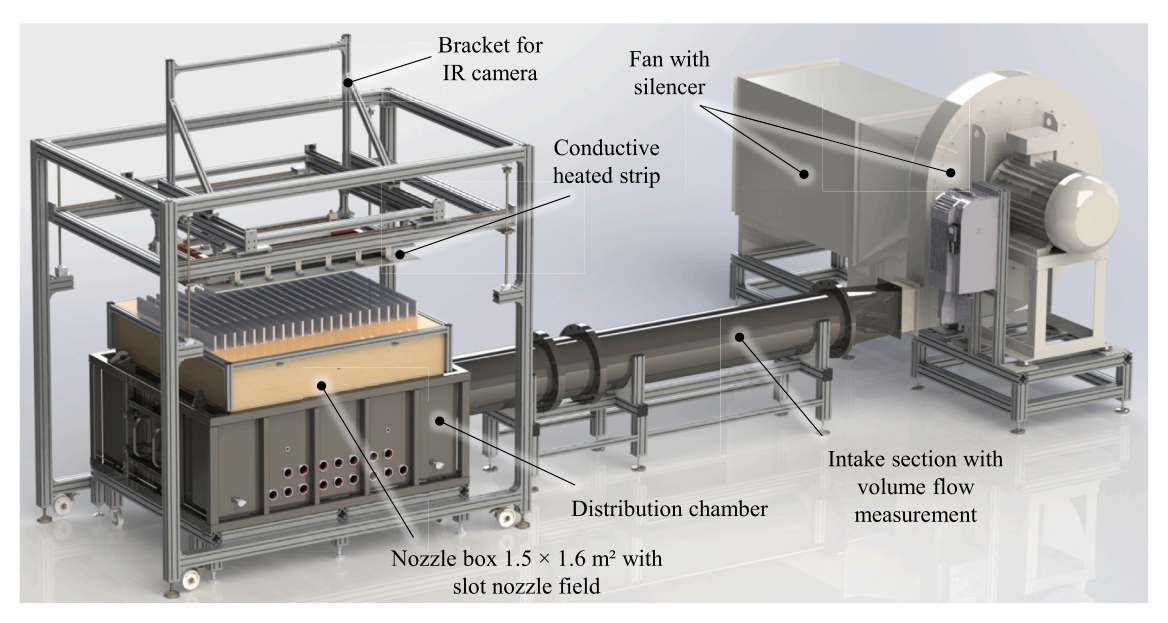


Fig. 2. Experimental setup to determine the heat transfer coefficient.

(2).

$$\dot{Q}_{gen} = \dot{Q}_{conv,force} + \dot{Q}_{conv,free} + \sum_{n=1}^{2} \dot{Q}_{n,rad} + \sum_{k=1}^{4} \dot{Q}_{k,cond}$$
 (2)

The amount of power supplied is equal to the heat dissipation of each pixel captured by the IR camera. The complete derivation can be found in the Trampe and Rademacher [19]. More information on the test rig can be found there, including full specifications of the equipment used and a detailed description of the method for determining the local heat transfer. The uncertainty of measurement for this method is $\varepsilon_h = \pm 4.4 \,\%$ respectively $\varepsilon_{Nu} = \pm 7.6 \,\%$ [19].

Table 1 summarises the test parameters used to determine the heat transfer and the nozzle geometries investigated. Note that the hydraulic diameter D_h of a round nozzle is equal to D, while for the slot nozzle, D_h is equal to D_h while for the slot nozzle, D_h is equal to D_h which is the differential pressure between the pressure at the nozzle exit D_h and the ambient pressure D_h which is the design of nozzle systems. It has therefore been kept the same for both nozzles. The slightly different nozzle exit velocities and Reynolds numbers are for geometric reasons. All data were obtained at a temperature of D_h = D_h = D_h consider the heat transfer and D_h the heat transfer is equal to D_h the heat transfer and D_h the heat transfer is equal to D_h the heat transfer and D_h the heat transfer is equal to D_h the heat transfer and D_h the heat transfer is equal to D_h the heat transfer and D_h the heat transfer is equal to D_h the heat transfer and the heat transfer is equal to D_h the heat transfer and the heat transfer is equal to D_h the heat transfer and the heat transfer is equal to D_h the heat transfer and D_h the heat transfer is equal to D_h the heat transfer is equal to

For the PIV measurements, a second setup was built up consisting of similar components as the heat transfer setup on a smaller scale, but with full optical accessibility. At the beginning of the inlet section a fan draws in ambient air and accelerates it into the inlet section, creating an even flow to the nozzle box. A measuring orifice and various pressure sensors are located in the inlet section to measure the volume flow and its temperature. Here, the tracer particles are also introduced into the fluid flow. A nozzle box with a volume of 550 x 400 x 400 mm³ is connected to the inlet section. Various nozzles can be mounted here. A plate above the nozzle outlet serves as the impinged surface. The PIV setup consists of a double frame camera (Imager CX2-16 LaVision GmbH, resolution 5312 x 3024 pixels) and a double pulsed Nd:YAG laser (Litron LPU 550, wavelength $\lambda = 532$ nm). This setup is shown in Fig. 3. The PIV measurements were carried out using the nozzle geometries and flow conditions listed in Table 1.

Each flow state was measured for 10 s. During this period, 800 double images were recorded, whereby the time interval Δt between two images at the same instant was set to $\Delta t = 5~\mu s$. The recorded particle patterns were analysed using DaVis 11 software provided by LaVision GmbH. From the 800 images an average image of the flow was generated. The spatial resolution is 32 x 32 pixels with an overlap of 75 %.

3. Experimental results

The experimental investigation of impingement jets from slot and round nozzles is required for determining the Nusselt Number Nu between fluid and metal strip. This parameter is used to design thermal processing plants. However, investigations of the heat transfer alone

lack information about the flow. This gap is filled in this work by supplementing the results with visualising the flow characteristics. The combined results of Nusselt number and flow characteristics provide a more complete understanding of heat transfer on impingement jets. The results obtained and conclusions drawn can be used to identify the strengths and limitations of numerical turbulence models.

3.1. Heat transfer coefficient

The results of the heat transfer measurements are based on the test parameters shown in Table 3. Fig. 4 a) illustrates the locally determined Nusselt number per pixel, where Fig. 4 b) shows the Nusselt number in the longitudinal direction through a SSN in cross section A-A. The measured local Nusselt numbers are given with a measurement uncertainty of $\varepsilon_{Nu} = \pm 7.6$ % (grey band).

The cross-section for the local Nusselt numbers is shown as an example, although it can be assumed to be the same for a slot nozzle over its entire length. The distribution of local Nusselt numbers of a slot nozzle is characterised by a maximum at the centre of the slot with Nu=143. Thereafter, the local Nusselt number decreases continuously with increasing distance from the centre of the slot nozzle. The outlet flow of the slot nozzle is laterally symmetrical. The locally determined Nusselt numbers per pixel for a single round nozzle is represented in Fig. 5 a) while Fig. 5 b) shows these Nusselt numbers in the longitudinal direction through the centre of the nozzle in section A–A.

A first maximum with $Nu \approx 200$ can be seen in the centre of the nozzle, which is subject to local fluctuations. The local fluctuations in the area of the stagnation point can be attributed to the oscillation of the impingement jet. This region is followed by a local minimum of Nu = 170 towards the nozzle wall, which is then again followed by a second local maximum of Nu = 210. The formation of two strong local maxima with increased heat transfer is typical for round nozzles. The distribution of the maxima and minima can be regarded as rotationally symmetrical. The flow corresponds to the characteristics expected from the studies for the single slot nozzle [10,23] and the round single nozzle [15,18,33].

Table 3Test parameters for determining the heat transfer.

Nozzle Geometry	SSN	SRN
Hydraulic Diameter D_h in mm	10	25
Nozzle Length L in mm	100	80
Strip Distance H in mm	50	50
Nozzle Box Pressure p in Pa	1,520	1,550
Nozzle Exit Velocity u in m/s	51.2	52.6
Nozzle Reynold Number Re	34,490	88,780

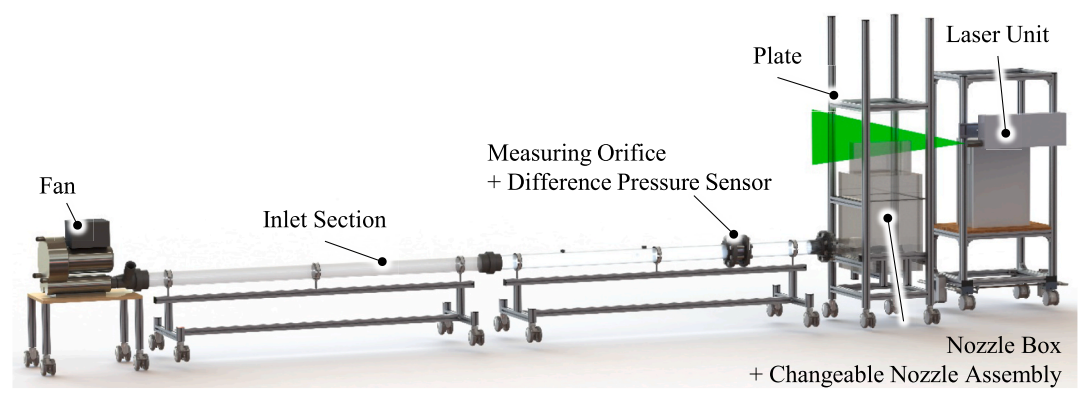


Fig. 3. Experimental setup to determine the velocity distribution in impingement jets using PIV.

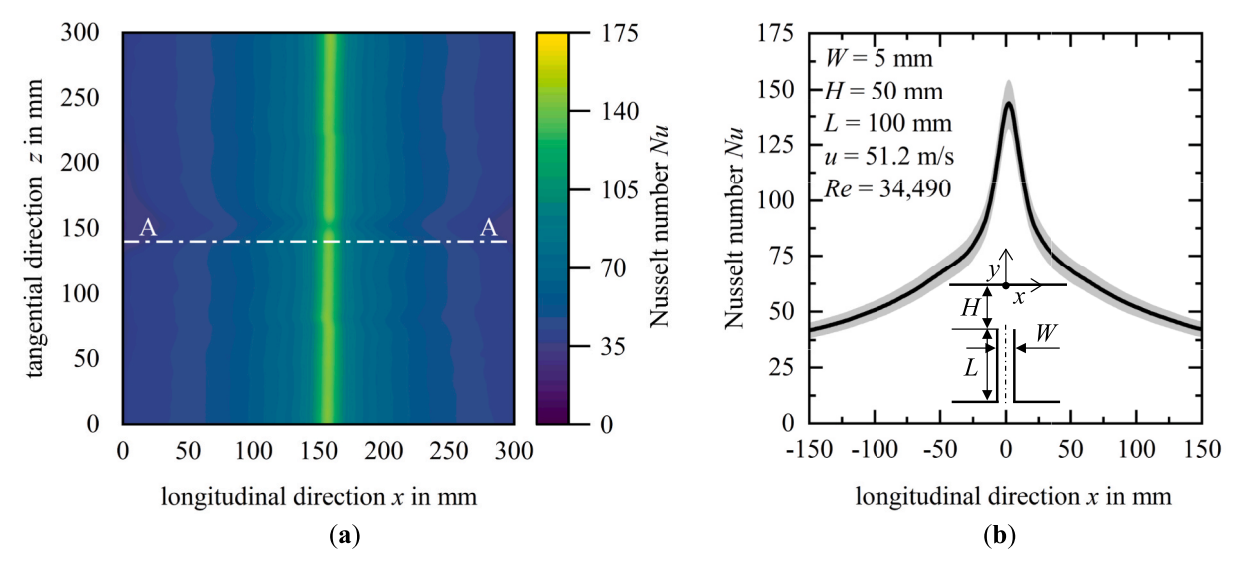


Fig. 4. A) Distribution of forced local nusselt numbers and b) nusselt numbers at section A–A through the centre of a SSN W = 5 mm at p = 1,520 Pa, u = 51.2 m/s, Re = 34,490, T = 25 °C.

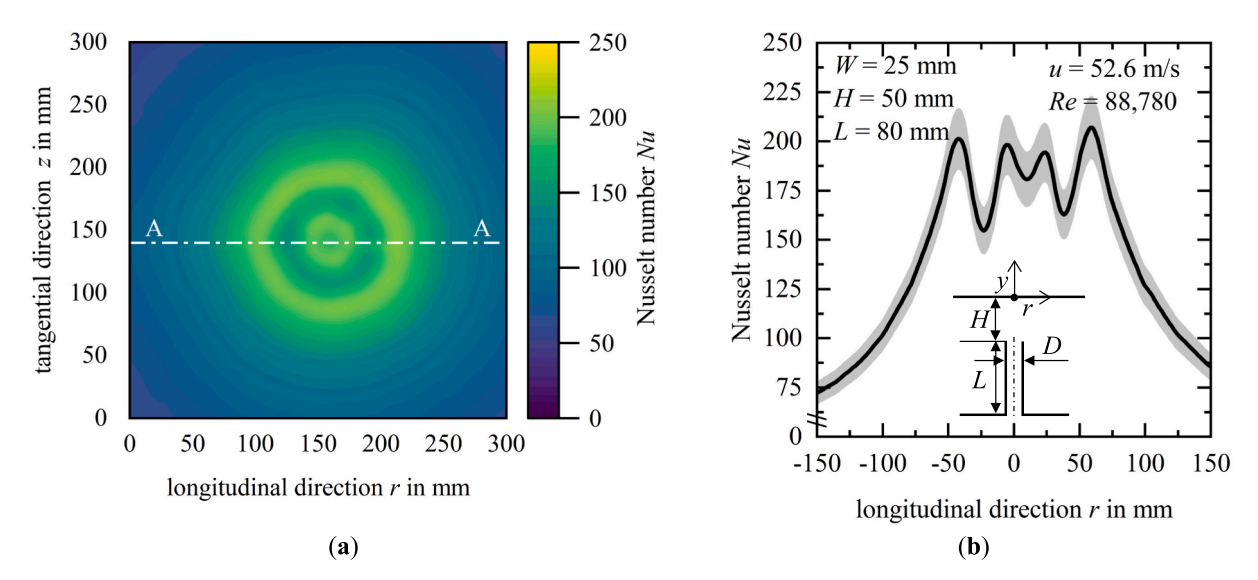


Fig. 5. A) Distribution of forced local nusselt numbers and b) nusselt numbers at section A-A through the centre of a SRN D=25 mm at p=1,550 Pa, u=52.6 m/s, Re=88,780, T=25 °C.

3.2. Flow characteristics

The velocity distribution of the impingement jets, determined by the PIV, shows their individual flow zones with different velocities. This method allows both the flow to be displayed for a defined point in time, e.g. to investigate the formation of vortices, and an averaged flow. The latter is used in this study. The time-averaged flow is more representative of the industrial application, as most thermal process plants are subject to a continuous process. Fig. 6 a) represents the average velocity distribution for a slot nozzle and Fig. 6 b) that of a round nozzle. The strip distance $H=50\,$ mm corresponds to Table 1.

The velocity distributions of the flow from the slot nozzle and the round nozzle are very similar. Immediately after the nozzle exit, a nozzle exit velocity of $u_{Exit,Slot}=51.2~\text{m/s}$ and $u_{Exit,Round}=52.6~\text{m/s}$ respectively is reached. As the distance from the nozzle outlet increases the free jet mixes with the ambient air and expands. As result the flow is slowed down. The stagnation region is clearly visible in both cases, as is the subsequent wall flow. In contrast to the slot nozzle, a coherent flow between the free jet region and the stagnation and wall region can be

recognised in the flow from the round nozzle. The uncertainty of the velocity distribution for the slot nozzle and the round nozzle is shown in Fig. 7. For both nozzles, the measurement standard deviation of the velocity is in the range of $\varepsilon_u=\pm~0$ m/s to $\varepsilon_u=\pm~1.5$ m/s depending on the flow region, calculated using DaVis 11 software.

The measurement uncertainty of the velocity when analysing the slot nozzle Fig. 7 a) shows that the uncertainty is $\varepsilon_u=\pm$ 0.8 m/s in the area of the mixture between the free jet and the ambient air, as well as in the wall jet. At the stagnation point, the uncertainty of the velocity is slightly higher with $\varepsilon_u=\pm$ 1.15 m/s, leading to the conclusion that areas with increased vorticity are more difficult to analyse accurately. Similar statements can be made about the measurement uncertainty of the velocity distribution of the round nozzle, Fig. 7 b). Same as before the highest measurement uncertainty ($\varepsilon_u=\pm$ 0.9 m/s) can be seen in the area of the mixing zone and the wall jet. However, the stagnation point is recorded with a significantly lower measurement deviation of $\varepsilon_u=\pm$ 0.35 m/s.

In addition to the speed-dependent measurement uncertainty, the specification of the measurement uncertainty in pixels is another

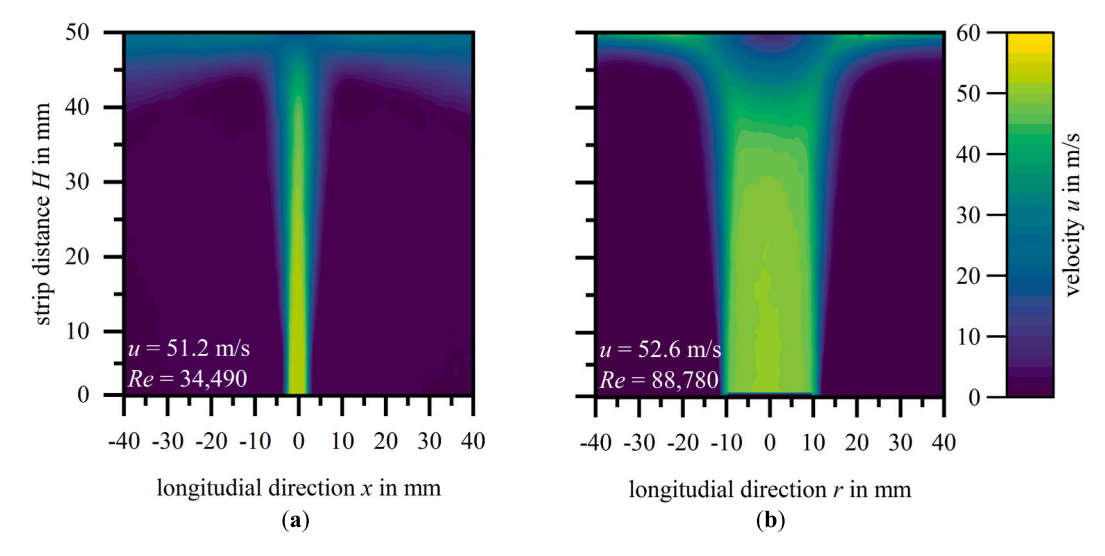


Fig. 6. Average velocity distribution of the a) SSN W=5 mm and b) SRN D=25 mm with H=50 mm.

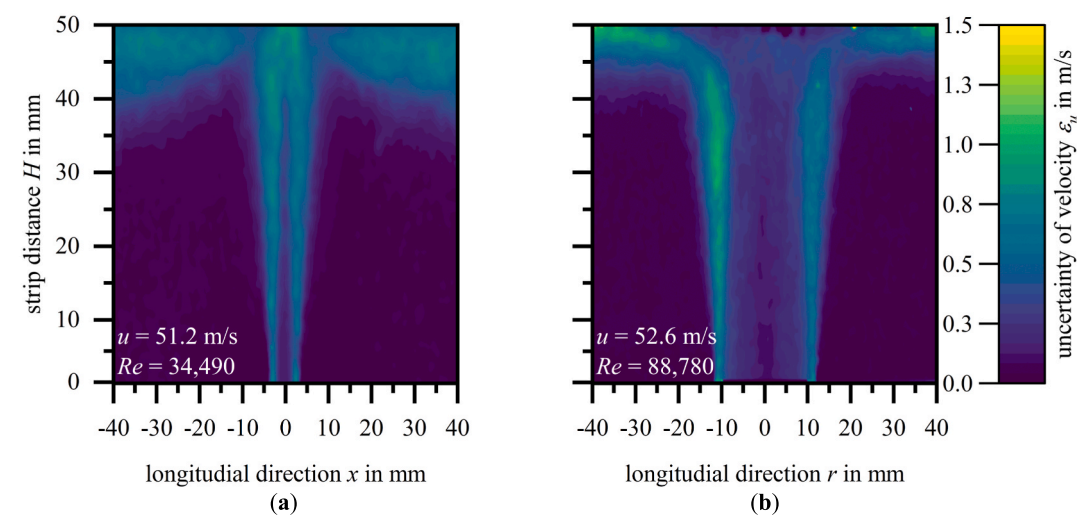


Fig. 7. Uncertainty in the velocity distribution of the a) SSN W = 5 mm and b) SRN D = 25 mm with H = 50 mm.

method for assessing the quality of PIV measurements which is an internationally recognise unit [37,38]. According to Wieneke, a value of 0.01 pixels is considered excellent and a value of 0.3 pixels is considered poor [37]. Analogue to the measurement uncertainty of the velocity distribution, the largest measurement deviations per pixel of the present investigations are in the area of large turbulence. When analysing the flow from the slot nozzle, the largest value is 0.18 pixels (stagnation point) and for the round nozzle 0.12 pixels (mixing region). In all other regions, the value is below 0.05 pixels, indicating that the measurements are of good quality.

For impingement jet flows, the Reynolds number Re is formed from the nozzle exit velocity u, the hydraulic diameter D_h and the kinematic viscosity ν , Eq. (3), whereby Re > 100 is sufficient to describe a jet flow turbulent [7].

$$Re = \frac{u \cdot D_h}{\nu} \tag{3}$$

This limit is clearly exceeded in the present work, Table 1, according to which it is a fully turbulent impingement jet flow. In this case, the turbulent kinetic energy k can be used as a quantitative measure of the turbulence intensity. The kinetic energy for a turbulent flow with time-averaged velocity components is mathematically defined as [39]:

$$k = \frac{1}{2} \cdot \left(\overline{u^2} \cdot \overline{v^2} \cdot \overline{w^2} \right) \tag{4}$$

The information on the distribution of the turbulent kinetic energy k of the impingement jet expands the understanding of the flow characteristics and provides a second representative variable for evaluating the numerical turbulence models. Fig. 8 a) shows the distribution of the turbulent kinetic energy for the slot nozzle and Fig. 8 b) for the round nozzle.

The distribution of the turbulent kinetic energy of the impingement jet of the slot nozzle shows many areas that are characterised by a high turbulent kinetic energy of $k > 70~\text{m}^2/\text{s}^2$. These include the mixing region, the stagnation region and the wall flow. The stagnation region is particularly noteworthy as the highest turbulent kinetic energy of $k = 75~\text{m}^2/\text{s}^2$ is present locally. Only in the centre area of the free jet the turbulent kinetic energy is $k < 15~\text{m}^2/\text{s}^2$. The jet expansion of both the free jet and the wall flow are clearly recognisable. In this region, the kinetic energy of the turbulent flow is higher within the impinging jet and then decreases as the contact with the ambient air increases.

The distribution of turbulent kinetic energy in the impingement flow of the round nozzle shows on average a lower turbulent kinetic energy. The free jet region without interaction is very pronounced and has a

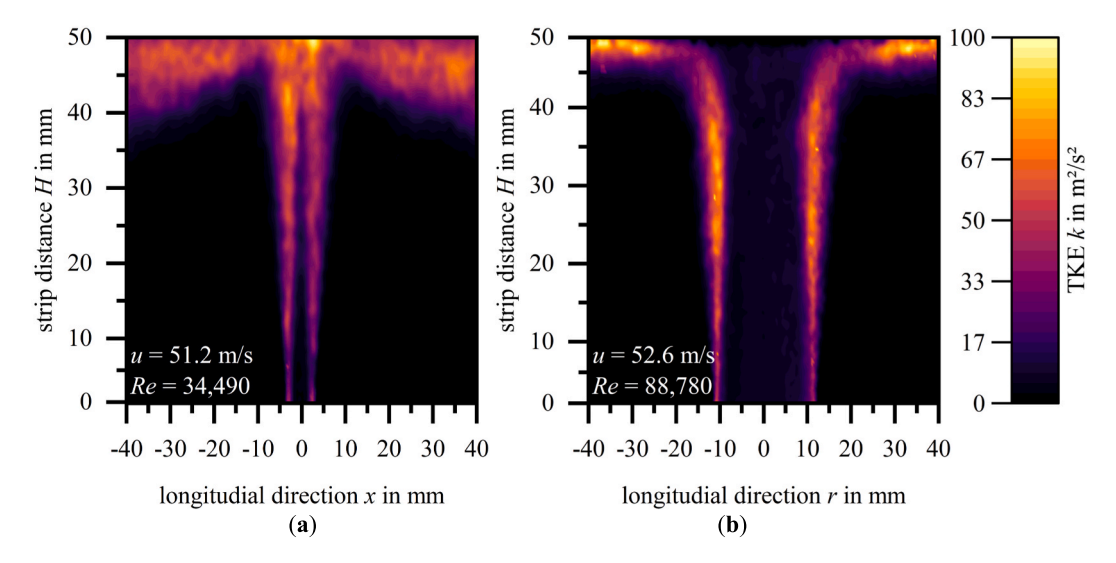


Fig. 8. Turbulent kinetic energy distribution of the a) SSN W = 5 mm and b) SRN D = 25 mm with H = 50 mm.

turbulent kinetic energy of $k < 10~\text{m}^2/\text{s}^2$. The stagnation region of the round nozzle impingement jet is also a region with low turbulent kinetic energy. The mixing region has a turbulent kinetic energy of $k = 30-60~\text{m}^2/\text{s}^2$. Only in the area of the wall flow at a distance of $r \pm 25~\text{mm}$ from the centre of the nozzle is the turbulent kinetic energy higher than $k > 70~\text{m}^2/\text{s}^2$.

4. Numerical methodology

The commercial software ANSYS Fluent 2024 R1 software is used for the numerical simulation of the impingement. The main focus is on the area close to the wall, as this is the most important area for convective heat transfer. The aim of this work is to demonstrate the strengths and weaknesses of heat transfer simulations by comparing the results with experimental local Nusselt numbers and flow visualisation using PIV.

4.1. Computational domain

The numerical calculations were carried out in a three-dimensional domain, which is shown in Fig. 9 with the corresponding boundary conditions. The nozzle inlet is defined as the velocity inlet (blue line), the two side faces as the pressure outlet (red lines). The constantan® strip (grey line) as well as the base and the nozzles (black lines) are all walls, whereby the is subjected to a constant het generation Φ analogous to the test rig. Therefore, the conditions described by Shukla [40] are met for this study.

In order to analyse the heat transfer on the constantan® strip and compare it with the measured data, a rake is placed over the constantan® strip. A rake is a fixed number of evaluation points along a

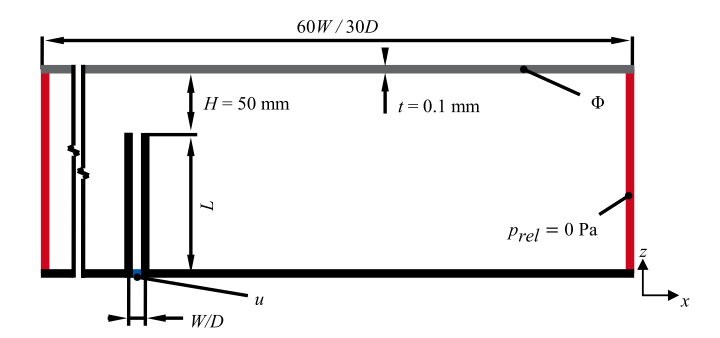


Fig. 9. Sketch of the fluid domain for a SSN; black/grey: wall, blue: velocity inlet, red: pressure outlet.

defined distance, where a local Nusselt number is calculated for each evaluation point. The number and spacing of the evaluation points correspond to the number of the pixels of the temperature measurement in the experiment, so the evaluation points are spaced 1.28 mm apart. With a measuring range of 300 mm, this corresponds to 244 evaluation points to be compared.

4.2. Mesh qualities

The mesh topology is generated based on the structured approach with a polyhedral mesh to maintain the highest mesh quality. It is then refined and adapted iteratively in regions with large velocity gradients. The area near the wall is also of particular interest. This is the region where convective heat transfer takes place. For a high prediction accuracy, it has been studied that the dimensionless wall distance y^+ , defined by Eq. (5), must be $y^+ \approx 1$ [11,41,42]. According to [35], the mesh even requires a dimensionless wall distance of $y^+ \approx 0.1$ in order to calculate a proper heat transfer.

$$\mathbf{y}^{+} = \frac{\rho \cdot \mathbf{u}_{T} \cdot \mathbf{y}}{\mu} \tag{5}$$

The key figures of the mesh dependency study are listed in Table 4. In addition to the total number of cells, these also include the dimensionless wall distances achieved. The meshes are evaluated in terms of the predicted average Nusselt number and the Nusselt number in the stagnation point. The minimum dimensionless wall distance y_{min}^+ is reached at the stagnation point. The generalised $k-\omega$ (GEKO) turbulence models was used for the grid dependence study.

Three meshes were investigated to find a suitable mesh that would provide accurate and computationally optimised numerical results. It was found that a stable solution was obtained with a mesh of 7.6 million cells. No further improvement was obtained by increasing the number of elements in the mesh, i.e. beyond a medium mesh size, the computational time and cost increase dramatically for a very small increase in the mean Nusselt number. The investigation of even coarser meshes than those shown here was not attempted as the dimensionless wall distance

Table 4Key figures of the mesh dependency study for the SSN.

Mesh	Number of cells	\mathcal{Y}_{min}^{+}	y_{max}^+	\mathcal{Y}_{ave}^{+}	Nu	Nu_{Stag}
Coarse	4.3 Mio.	0.9	2.5	1.4	446	172
Medium	7.6 Mio.	0.7	1.9	1.1	441	171
Fine	15.3 Mio.	0.4	1.3	0.7	447	168

already exceeds the specifications for the coarse mesh. Therefore, the medium mesh of 7.6 million cells was selected for further investigation. The mesh refinement technique described above was also applied to the fluid domain of the single round nozzle.

4.3. Turbulence modelling

The different flow velocities and the associated vortex formation along the jet are the main challenges in modelling impingement flows. A pre-selection of turbulence models was based on previous Reynold-Averaged Navier-Stokes (RANS) simulations, Section 1. The $k-\omega$ SST (Shear Stress Transport) and generalised k– ω (GEKO) turbulence models were chosen because of their low computational cost and good agreement in simulating impingement jets. The $k-\omega$ SST model is based on the $k-\omega$ standard model in the boundary layer region. This two-equation model solves one transport equation, each for the kinetic energy k and the vortex frequency ω . In the free jet region, the k– ω SST model behaves like a $k-\varepsilon$ model with good convergence rates. The combination of the standard $k-\omega$ and $k-\varepsilon$ model has the advantage that both, the near wall region and the free jet region, can be modelled in a meaningful way. The GEKO turbulence model is also based on the two equations of the $k-\omega$ model, but has six additional independent parameters that can be adjusted without affecting the fundamentals of the model [43].

The Reynold Stress Model (RSM), stress - ω model combination, was chosen as the third turbulence model. Unlike the previous turbulence models, each respective Reynolds stress is described by a single equation. This eliminates the generalised assumption of isotropic turbulence, but increases the computational effort [43].

5. Validating numerical results

The experimental data leads to a better understanding of the convective heat transfer of impingement jets. This serves as a basis for optimising the numerical modelling of impingement jets and for critically reviewing numerical results. In a first step, the experimentally determined local Nusselt numbers of the longitudinal cross section A-A are compared with the calculated Nusselt numbers of the numerical models. Fig. 10 a) shows the local distribution of the Nusselt numbers in the cross-section, determined experimentally and numerically for a) a single slot nozzle and Fig. 10 b) a single round nozzle. Three turbulence models shear stress transport (SST) $k\text{-}\omega$ turbulence model, generalized $k\text{-}\omega$ (GEKO) turbulence model and Reynolds Stress Model (RSM), were selected. The experimentally determined data are given with the calculated measurement deviation of $\epsilon_{\rm Nu} \pm 7.6$ %.

The comparison of the experimentally determined Nusselt numbers

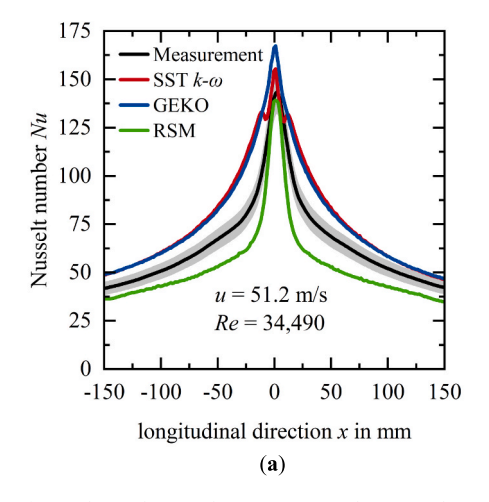
with the numerically calculated Nusselt numbers shows that no numerical model completely reproduces the measured data. The average deviation of all numerical calculations is about 19 % for the slot nozzle and 34 % for the round nozzle, whereby the RSM model achieves an average of 11 % but incorrectly depicts the typical pattern. In particular, the characteristic heat transfer patterns are not reproduced by any model, so that the SST k- ω turbulence model specifies a second secondary maximum for the slot nozzle that does not even exist.

The SST k- ω and GEKO turbulence models tend to overestimate the solution. In the present study, the deviation is greater than in the comparative studies [23,27], which may be due to the significantly higher Reynolds number. In contrast to Barata's study [27], the RSM model in this study achieves a high degree of accuracy at the stagnation point. Thereafter, the solution is underestimated, which is also not observed in Barata's study [27]. The prediction accuracy of the SST k- ω and GEKO turbulence models is in good agreement with Menzler's results [28]. It can be concluded that the prediction accuracy is strongly dependent on the Reynolds number and tends to decrease at high Reynolds numbers.

In agreement with the present results, [18,32,34,36] represent that the numerical turbulence models overestimate the solution overall. All investigations show a decrease in heat transfer at the stagnation point for the SST k- ω and GEKO turbulence models. This is not observed for the RSM model with the stress - ω model combination [34], which is consistent with the available results. Analogous to the results for the single slot nozzle, it can be seen that the prediction accuracy decreases with increasing Reynolds number.

The preliminary finding, based on the investigative work undertaken, indicates that the outcomes of the research field are predominantly validated. Nevertheless, it is evident that the predictive precision of numerical models is diminished at elevated Reynolds numbers. A comparison is made between the flow patterns exhibited by the numerical calculations and the measured velocity and turbulent kinetic energy distributions obtained from the PIV measurements. This is undertaken to comprehend the reasons why the turbulence models are unable to accurately replicate the patterns of the local Nusselt number. Fig. 11 shows the comparison between the calculated velocity distributions of the different numerical turbulence models and the experimental PIV measurement of the single slot nozzle. Both the experimental and numerical results demonstrate that the existing impingement flows can be assumed to be symmetrical. Therefore, only the results along the positive longitudinal direction are compared in the following.

The simulated velocities of the impingement jet by the GEKO and turbulence model are very similar and are similar to those of the PIV measurement. The RSM model predicts all velocities significantly higher



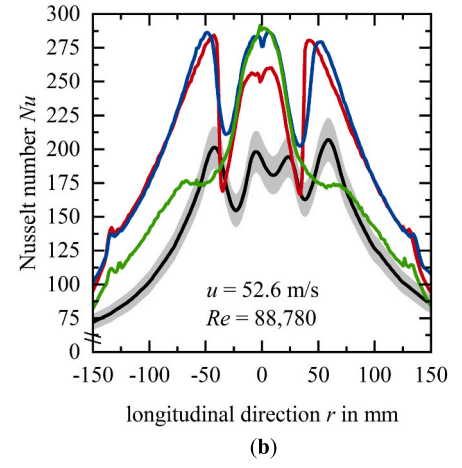


Fig. 10. Local distribution of Nusselt numbers in the cross-section determined experimentally and numerically for a) SSN W = 5 mm at p = 1,520 Pa, u = 51.2 m/s, Re = 34,490, T = 25 °C and b) SRN D = 25 mm at p = 1,550 Pa, u = 52.6 m/s, Re = 88,780, T = 25 °C with T = 50 mm.

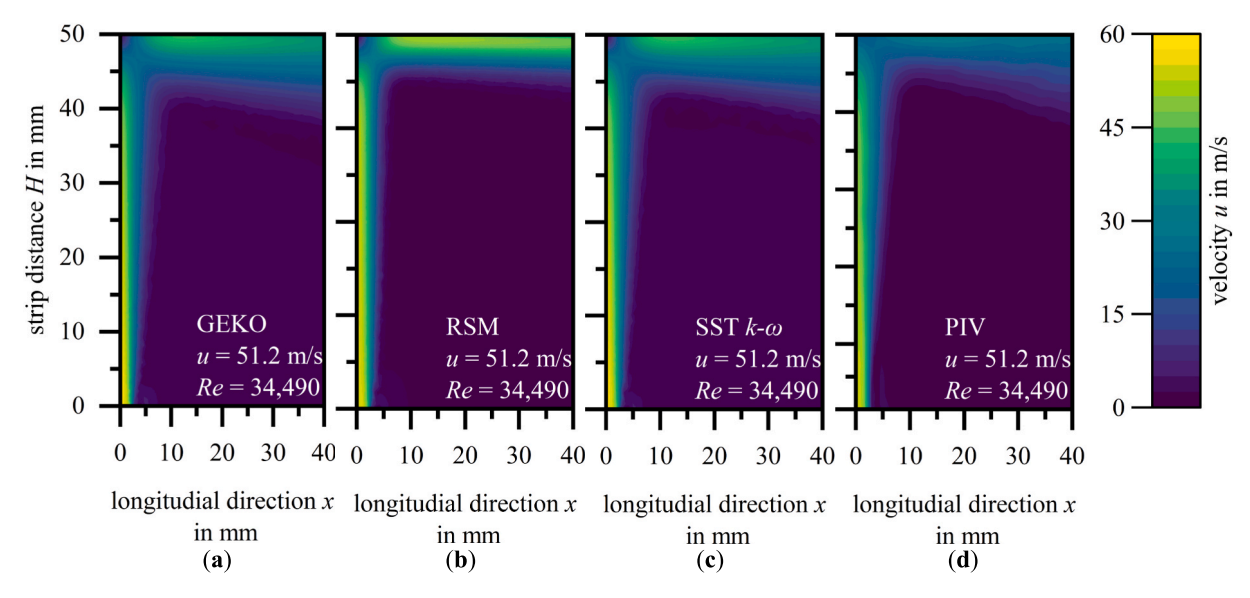


Fig. 11. Comparison between the average velocity distribution of the a) GEKO b) RSM c) SST $k-\omega$ turbulence model and d) PIV measurement for the SSN W=5 mm at p=1,520 Pa, u=51.2 m/s, Re=34,490 with H=50 mm.

than the PIV measurement shows. The transition between free jet and wall flow is also modelled differently, here the transition appears to be smoother than in the PIV and GEKO or SST k- ω turbulence model. The flow characteristics of the PIV measurement are qualitatively consistent with Senter's [44] and Benmouhoub's [23] observations. The turbulent kinetic energy distribution of the slot nozzle impingement jet is compared in Fig. 12 for the numerical turbulence models and the PIV measurement. The scaling of the TKE was subsequently limited to $k = 60 \text{ m}^2/\text{s}^2$, as the predicted turbulent kinetic energies of the turbulence models are significantly lower. A visual comparison is only possible with a lower scaling, even if the turbulent kinetic energy of the PIV measurement exceeds these values, compare Fig. 8.

The GEKO and SST k- ω turbulence models reproduce the turbulent kinetic energy of the impingement jet most accurately compared to the PIV measurement. Both numerical turbulence models calculate a lower turbulent kinetic energy at the stagnation point and an equally high turbulent kinetic energy in the free jet and in the wall jet, compared to the PIV measurement. Before the turbulent kinetic energy decreases in

the direction of the ambient air, there is a narrow band with maximum turbulent kinetic energy in the wall jet region. A clear difference in the calculation of the turbulent kinetic energy can be seen in the turbulence model RSM with only one fifth of the energy. On average, the turbulent kinetic energy in the impingement jet is in this case only $k \approx 10 \text{ m}^2/\text{s}^2$, but there is a local maximum of $k = 20 \text{ m}^2/\text{s}^2$ at the stagnation point. It might be assumed that the RSM turbulence model would predict a higher heat transfer, as it calculates higher velocities in the wall jet. However, this is not the case. This may be due to the under-calculated turbulent kinetic energy, which is only one fifth of the PIV measurement.

The results of the numerical and experimental investigations of the round nozzle are presented in the same way as those of the slot nozzle. The distribution of the mean velocity based on the numerical turbulence models and the PIV measurement is presented comparatively in Fig. 13.

There are no noticeable differences between the results of the different turbulence models, Fig. 13 a) - c), and those of the PIV measurement, Fig. 13 d). The studies by Rasheed [36] and Dairay [45] indicate the same flow characteristics as shown here. This leads to the

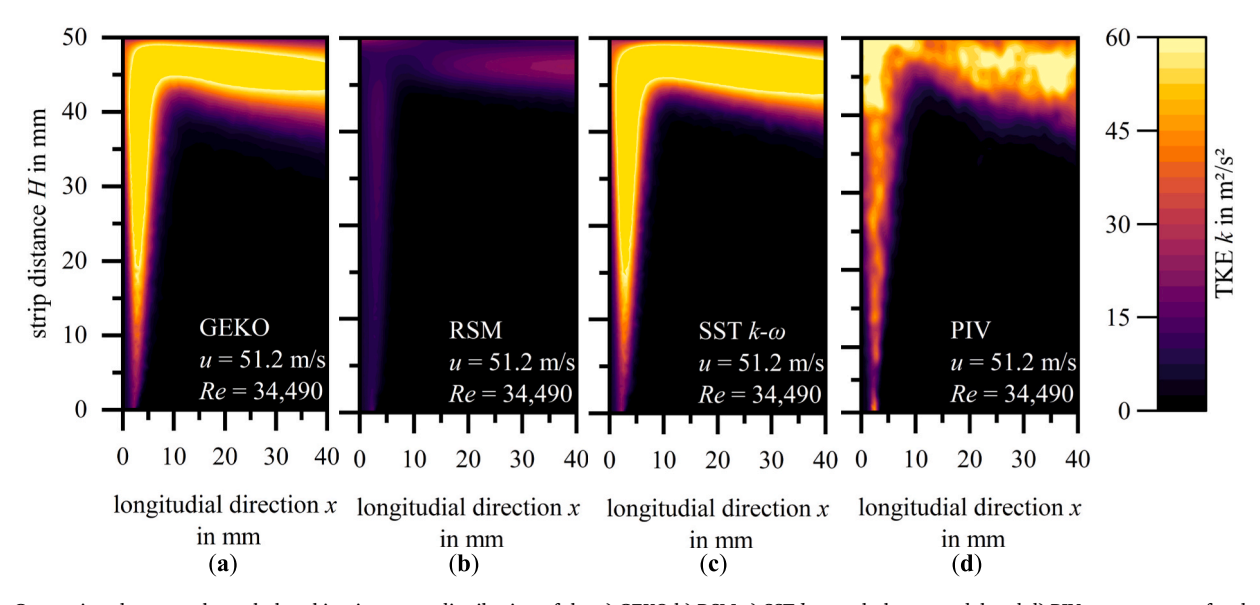


Fig. 12. Comparison between the turbulent kinetic energy distribution of the a) GEKO b) RSM c) SST $k-\omega$ turbulence model and d) PIV measurement for the SSN W=5 mm at p=1,520 Pa, u=51.2 m/s, Re=34,490 with H=50 mm.

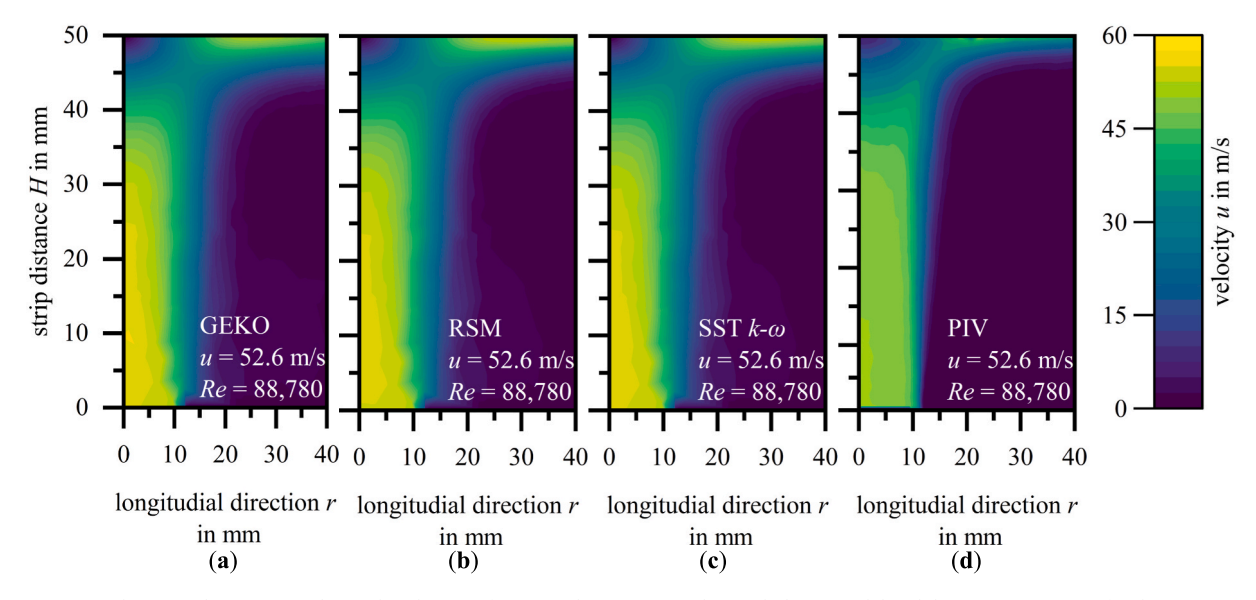


Fig. 13. Comparison between the average velocity distribution of a) GEKO b) RSM c) SST k– ω turbulence model and d) PIV measurement for the SRN D=25 mm at p=1,550 Pa, u=52.6 m/s, Re=88,780 with H=50 mm.

conclusion that it is not a challenge for turbulence modelling to correctly reproduce the flow velocities and directions even at high Reynolds numbers. Fig. 14 shows the distribution of the turbulent kinetic energy of the impingement jet of a round nozzle calculated by the numerical turbulence models, Fig. 14 a) – c), and the PIV measurement, Fig. 14 d).

In contrast to the calculation of the velocity distribution, there are clear differences between the individual numerical turbulence models for the calculation of the turbulent kinetic energy of the round nozzle. The PIV measurement shows that the highest turbulent kinetic energy is always in the mixing region and merges smoothly into the wall flow. The stagnation point does not show any increased turbulent kinetic energy. This observation was also made by Dairay [45].

The GEKO turbulence model, Fig. 14 a), predicts a homogeneous distribution of turbulent kinetic energy in the mixing zone. After the impingement jet has passed through the stagnation zone, the turbulent kinetic energy increases in the transition to the wall flow, where it reaches its maximum of $k \approx 60 \text{ m}^2/\text{s}^2$. Comparing this pattern with the results of the SST k– ω turbulence model, Fig. 14 c), the same structure

can be seen. However, the maximum turbulent kinetic energy in the wall flow is only $k \approx 40 \text{ m}^2/\text{s}^2$. The RSM turbulence model, Fig. 14 b), calculates the turbulent kinetic energy in the free jet and in the mixing region as $k=6.5 \text{ m}^2/\text{s}^2$ and is therefore significantly lower than the results of the GEKO and SST k– ω turbulence models and the PIV measurement. However, the turbulent kinetic energy in the near wall region from the stagnation point to the pronounced wall flow is predicted to be $k\approx 20 \text{ m}^2/\text{s}^2$ at all locations.

Dairay [45] and Yüksekdağ [32] also observed that there are areas of high turbulent kinetic energy at the edge of the jet and also at the widening of the wall jet. The zone of high turbulent kinetic energy in the wall jet is more pronounced in this study and the difference between the turbulent kinetic energy in the mixed zone of the free jet and the wall jet is greater than in Dairay's study [45].

6. Conclusion

In industrial thermal processing plants, metal strips are quenched in

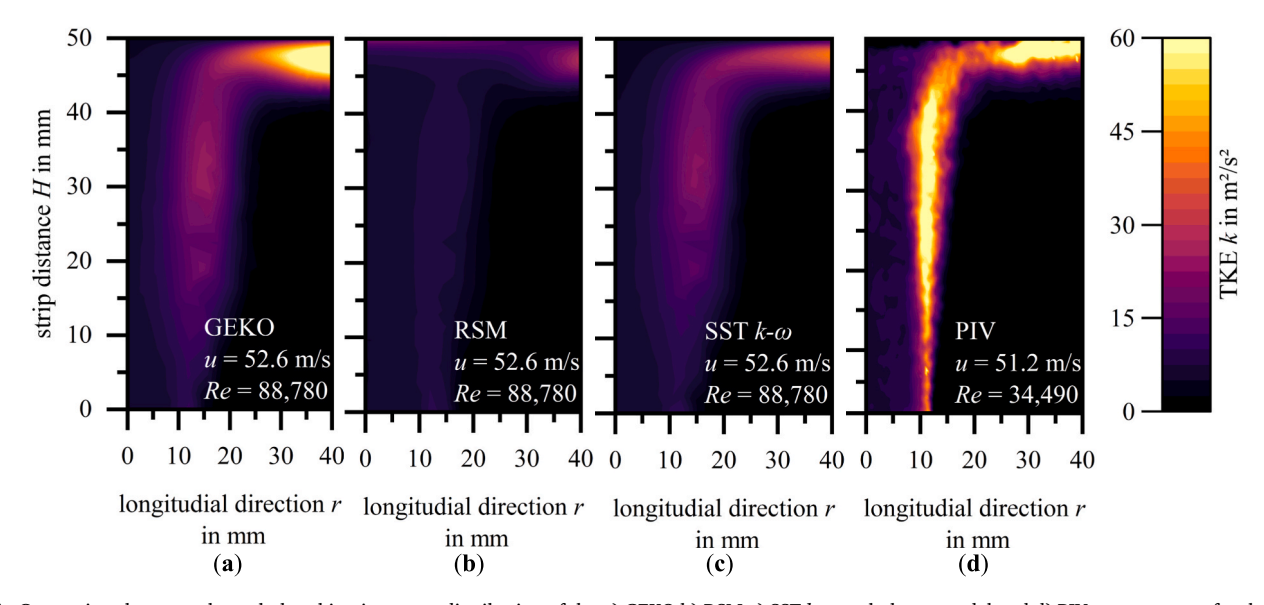


Fig. 14. Comparison between the turbulent kinetic energy distribution of the a) GEKO b) RSM c) SST $k-\omega$ turbulence model and d) PIV measurement for the SRN $D=25\,$ mm at $p=1,550\,$ Pa, $u=52.6\,$ m/s, $Re=88,780\,$ with $H=50\,$ mm.

cooling zones by impingement jets, with convection being the dominant heat transfer mechanism. To generate the impingement jets, gas is accelerated through a nozzle system and directed onto the material surface, resulting in rapid and uniform cooling. The present work involves the experimental investigation of the local Nusselt number and PIV measurements to visualise the flow of impingement jets. A single slot (W=5 mm) and a single round nozzle (D=25 mm) are used.

These experimental methods form the basis for the evaluation of numerical turbulence models. Turbulence models are used to approximate the flow of the impingement jet with the following models discussed in this work: SST k- ω model, Generalised k- ω (GEKO) model and the Reynolds Stress Model. The investigations are carried out at a nozzle exit velocity of $u \approx 51$ m/s ($Re_{Slot} = 34,490$, $Re_{Round} = 88.780$), being a typical exit velocity of industrial nozzle systems used for the heat treatment. Compared to other studies, the prediction accuracy is lower due to the high Reynolds numbers. The flow velocities are correctly modelled, but the turbulent kinetic energy is poorly predicted compared to the PIV measurement.

This method has proved its utility in demonstrating the strengths and limitations of each turbulence model. Comparison with other studies using comparable geometries but lower Reynolds numbers showed similar flow characteristics. However, this study has shown that the prediction accuracy deteriorates at higher Reynolds numbers, indicating the need for further research. In order to be able to make reliable statements about the prediction accuracy of different turbulence models at high Reynolds numbers, it is therefore necessary to build up a larger database with different flow velocities.

This database must be in particular used to improve the prediction of secondary peaks in the numerical modelling and their agreement with the measurement results of impingement jets. The occurrence of the typical flow pattern with different peaks has not yet been conclusively clarified from a phenomenological point of view. The approach taken in this work to describe the occurrence of secondary peaks in terms of turbulent kinetic energy is promising but requires further investigation [35,46,47]. This approach can also be used to further develop existing turbulence models and adapt them to the requirements of impingement jet modelling.

Declaration of competing interest

The authors declare that they have no known competing financial interests or personal relationships that could have appeared to influence the work reported in this paper.

Data availability

Data will be made available on request.

References

- C. Kramer, M. Hansen, Gas jet floatation for the touchless cooling of sensitive stainless steel strips in strip annealing lines, *Heat Processing* (2006) 24–26.
- [2] W. Schütt, Jet-heating-durchlauföfen fur die erwärmung und wärmebehandlung von schmiede- und gussteilen aus aluminium sowie stahlbauteilen bis 800 °C: sonderheft energieeffizienz, Gaswärme International (2009) 1–4.
- [3] SMS group GmbH. Annealing and galvanizing lines. Available online: https://www.sms-group.com/de-de/plants/annealing-and-galvanizing-lines-for-steel (accessed on 7 February 2025).
- [4] L. Wang, J.G. Speer, Quenching and partitioning steel heat treatment, Metallogr. Microstruct. Anal. 2 (2013) 268–281, https://doi.org/10.1007/s13632-013-0082-8.
- [5] B. Liscic, Quenching theory and technology, 2nd ed., Chapman and Hall/CRC, Baton Rouse, 2010.
- [6] T.L. Bergman, A.S. Lavine, F.P. Incropera, D.P. Dewitt, Fundamentals of heat and mass transfer, John Wiley & Sons, 2011.
- [7] VDI e.V. VDI-Wärmeatlas; Springer Berlin Heidelberg: Berlin, Heidelberg, 2013, ISBN 978-3-642-19980-6.
- [8] Praxishandbuch Thermoprozesstechnik Band II: Anlagen, Komponenten, Sicherheit: Durchlauföfen für nicht rostenden Stahl und Kohlenstoffstahl; Pfeifer, H.; Nacke, B.; Beneke, F., Eds., 2nd ed.; Vulkan-Verlag GmbH: Essen, 2011.
- [9] E. Hilgeroth, Wärmeübergang bei düsenströmung senkrecht zur austauschfläche, Chem. Ing. Tech. (1965) 1264–1272.

- [10] Martin, H. Heat and Mass Transfer between Impinging Gas Jets and Solid Surfaces. Advances in Heat Transfer Volume 13; Elsevier, 1977; pp 1–60, ISBN 9780120200139.
- [11] D. Menzler, Konvektionskühlsysteme für leichtmetallhalbzeuge, RWTH Aachen University, Aachen, 1992.
- [12] L. Florschuetz, C. Truman, D. Metzger, Streamwise flow and heat transfer distributions for jet array impingement with crossflow, J. Heat Transfer (1981).
- [13] C. Kramer, K. Berns, Wärmeübergang bei interferenz von prall-und tangentialströmung, Gaswärme International (1988) 378–384.
- [14] A.M. Huber, R. Viskanta, Effect of jet-jet spacing on convective heat transfer to confined, impinging arrays of axisymmetric air jets, *Int. J. Heat Mass Transf.* 37 (1994) 2859–2869, https://doi.org/10.1016/0017-9310(94)90340-9.
- [15] V. Katti, S.V. Prabhu, Influence of spanwise pitch on local heat transfer distribution for in-line arrays of circular jets with spent air flow in two opposite directions, Exp. Therm Fluid Sci. 33 (2008) 84–95, https://doi.org/10.1016/j. expthermflusci.2008.07.004.
- [16] A. Gangoli Rao, L. Yeshayahou, M. Kitron-Belinkov, Heat Transfer Characteristics of a Multiple Jet Impingement System 1 (2009) 314–328.
- [17] T.S. O'Donovan, D.B. Murray, Jet impingement heat transfer Part I: mean and root-mean-square heat transfer and velocity distributions, Int. J. Heat Mass Transf. 50 (2007) 3291–3301, https://doi.org/10.1016/j.ijheatmasstransfer.2007.01.044.
- [18] S. Alimohammadi, D.B. Murray, T. Persoons, Experimental validation of a computational fluid dynamics methodology for transitional flow heat transfer characteristics of a steady impinging jet, J. Heat Transfer 136 (2014) doi:10.1115/ 1.4027840
- [19] E. Trampe, N. Rademacher, M. Wulfmeier, D. Büschgens, H. Pfeifer, A high-resolution method for the experimental determination of the heat transfer coefficients of industrial nozzle systems in heat treatment plants, *Appl. Sci.* 14 (2024) 3024, https://doi.org/10.3390/app14073024.
- [20] L. Dhruw, H.B. Kothadia, A.K. Rajagopal, Local and area average Nusselt number correlation for a circular impinging jet over a flat plate, *J. Therm. Anal. Calorim* 148 (2023) 14031–14050, https://doi.org/10.1007/s10973-023-12593-4.
- [21] C.D. Argyropoulos, N.C. Markatos, Recent advances on the numerical modelling of turbulent flows, App. Math. Model. 39 (2015) 693–732, https://doi.org/10.1016/j. apm 2014 07 001
- [22] Zuckerman, N.; Lior, N. Jet Impingement Heat Transfer: Physics, Correlations, and Numerical Modeling; Elsevier, 2006; pp 565–631, ISBN 9780120200399.
- [23] D. Benmouhoub, A. Mataoui, Computation of heat transfer of a plane turbulent jet impinging a moving plate, *Therm. Sci.* 18 (2014) 1259–1271, https://doi.org/ 10.2298/TSCI111027101B.
- [24] A.M. Achari, M.K. Das, Conjugate heat transfer study of a turbulent slot jet impinging on a moving plate, *Heat Mass Transf.* 53 (2017) 1017–1035, https://doi. org/10.1007/s00231-016-1873-7.
- [25] Shashikant Pawar; Devendra Kumar Patel. NUMERICAL STUDY OF CONJUGATE HEAT TRANSFER DUE TO IMPINGEMENT OF TURBULENT SLOT JET ONTO A MOVING FLAT PLATE. In . 5 th International Conference on Computational Methods for Thermal Problems (ThermaComp2018), 2019.
- [26] P.K. Kadiyala, H. Chattopadhyay, Numerical analysis of heat transfer from a moving surface due to impingement of slot jets, *Heat Transfer Eng.* 39 (2018) 98–106, https://doi.org/10.1080/01457632.2017.1288045.
- [27] B. Barata, J. Navalho, J. Pereira, RANS simulations of plane impinging jets: On the influence of plate velocity in the Nusselt number secondary peak, *Therm. Sci.* 27 (2023) 4947–4960, https://doi.org/10.2298/TSCI230206127B.
- [28] J.E. Menzler, M. Klusmann, M. Wulfmeier, D. Büschgens, H. Pfeifer, Simulation of gas jet impingement cooling in continuous heat treatment lines with the ANSYS GEKO turbulence model*, HTM J. Heat Treatment Mater. 78 (2023) 91–104, https://doi.org/10.1515/htm-2022-1042.
- [29] Barbosa, F.V.; Teixeira, Senhorinha F. C. F.; Teixeira, J.C.F. Numerical Analysis of Single Jet Impinging a Flat and Non-flat Plate. In *Computational Science and Its Applications – ICCSA 2020*, 20th International Conference, Cagliari, Italy, July 1–4, 2020, Proceedings, Part V. International Conference on Computational Science and Its Applications; Gervasi, O., Murgante, B., Misra, S., Garau, C., Blečić, I., Taniar, D., Apduhan, B.O., Rocha, A.M.A.C., Tarantino, E., Torre, C.M., Karaca, Y., Eds.; Springer International Publishing; Imprint Springer: Cham, 2020; pp 487–495, ISBN 978-3-030-58814-4.
- [30] J.W. Baughn, A.E. Hechanova, X. Yan, An experimental study of entrainment effects on the heat transfer from a flat surface to a heated circular impinging jet, J. Heat Transfer 113 (1991) 1023–1025, https://doi.org/10.1115/1.2911197.
- [31] J.W. Baughn, S. Shimizu, Heat transfer measurements from a surface with uniform heat flux and an impinging jet, *J. Heat Transfer* 111 (1989) 1096–1098, https://doi.
- [32] R. Yüksekdağ, D. Koçak, U. Şentürk, Prediction of heat transfer for a single round jet impingement using the GEKO turbulence model, *Int. J. Heat Fluid Flow* 109 (2024) 109538, https://doi.org/10.1016/j.ijheatfluidflow.2024.109538.
- [33] M. Draksler, B. Končar, Analysis of heat transfer and flow characteristics in turbulent impinging jet, *Nucl. Eng. Des.* 241 (2011) 1248–1254, https://doi.org/ 10.1016/j.nucengdes.2010.03.037.
- [34] K. Petera, Turbulent heat transport and its anisotropy in an impinging jet, The European Phys. J. Conf. 92 (2015) 2063, https://doi.org/10.1051/epjconf/ 20159202063.
- [35] A. Chitsazan, G. Klepp, B. Glasmacher, Numerical prediction of the second peak in the nusselt number distribution from an impinging round jet, *IJHT* 39 (2021) 1243–1252, https://doi.org/10.18280/ijht.390422.
- [36] A. Rasheed, U. Allauddin, H.M. Ali, M. Uzair, P.G. Verdin, Y.H. Siddiqui, Heat transfer and fluid flow characteristics investigation using detached ribs in an

- axisymmetric impinging jet flow, *J. Therm. Anal. Calorim.* 147 (2022) 14517–14537, https://doi.org/10.1007/s10973-022-11640-w.
- [37] B. Wieneke, PIV uncertainty quantification from correlation statistics, Meas. Sci. Technol. 26 (2015) 74002, https://doi.org/10.1088/0957-0233/26/7/074002.
- [38] D.R. Neal, A. Sciacchitano, B.L. Smith, F. Scarano, Collaborative framework for PIV uncertainty quantification: the experimental database, *Meas. Sci. Technol.* 26 (2015) 74003, https://doi.org/10.1088/0957-0233/26/7/074003.
- [39] Pope, S.B. Turbulent flows, 1. publ., 12. print; Cambridge Univ. Press: Cambridge, 2015, ISBN 9780521591256.
- [40] A. Shukla, A. Dewan, Flow and thermal characteristics of jet impingement: comprehensive review, *IJHT* 35 (2017) 153–166, https://doi.org/10.18280/ iihr 350121
- [41] Analysis of turbulent flows with computer programs; Cebeci, T., Ed., 3. ed.; Butterworth-Heinemann: Oxford, 2013, ISBN 978-0-08-098335-6.
- [42] M. Kadivar, D. Tormey, G. McGranaghan, A review on turbulent flow over rough surfaces: fundamentals and theories, *Int. J. Therm.* 10 (2021) 100077, https://doi. org/10.1016/j.ijft.2021.100077.

- [43] Ansys®, F. Ansys Fluent Theory Guide 2023.
- [44] J. Senter, C. Solliec, Flow field analysis of a turbulent slot air jet impinging on a moving flat surface, *Int. J. Heat Fluid Flow* 28 (2007) 708–719, https://doi.org/ 10.1016/j.ijheatfluidflow.2006.08.002.
- [45] T. Dairay, V. Fortuné, E. Lamballais, L.E. Brizzi, LES of a turbulent jet impinging on a heated wall using high-order numerical schemes, *Int. J. Heat Fluid Flow* 50 (2014) 177–187, https://doi.org/10.1016/j.ijheatfluidflow.2014.08.001.
- [46] den Ouden, C.; Hoogendoorn, C.J. LOCAL COHVECTIVE-HEAT-TRANSFER COEFFICIENTS FOR JETS IMPINGING ON A PLATE; EXPERIMENTS USING A LIQUID-CRYSTAL TECHNIQUE. In Proceeding of International Heat Transfer Conference 5. International Heat Transfer Conference 5, Tokyo, Japan, 9/3/1974 -9/7/1974; Begellhouse: Connecticut, 1974 - 1974; pp 293–297.
- [47] V. Narayanan, J. Seyed-Yagoobi, R.H. Page, An experimental study of fluid mechanics and heat transfer in an impinging slot jet flow, *Int. J. Heat Mass Transf.* 47 (2004) 1827–1845, https://doi.org/10.1016/j.ijheatmasstransfer.2003.10.029.